Spin-isovector giant resonances induced by (n,p) reactions on heavy nuclei

S. A. Long,[1] B. M. Spicer,[1] K. J. Raywood,[2] R. Abegg,[2,*] W. P. Alford,[5] A. Celler,[2,4] D. Frekers,[2] P. E. Green,[2] O. Häusser,[2,4] R. L. Helmer,[2] R. S. Henderson,[2] K. H. Hicks,[2,7] K. P. Jackson,[2] R. G. Jeppesen,[4] N. S. P. King,[6] C. A. Miller,[2] M. A. Moinester,[3] V. C. Officer,[1] G. G. Shute,[1] A. Trudel,[2] M. C. Vetterli,[4] A. I. Yavin,[3] and S. Yen[2]

[1]*School of Physics, University of Melbourne, Parkville, Victoria, Australia 3052*

[2]*TRIUMF, 4004 Wesbrook Mall, Vancouver, British Columbia, Canada V6T 2A3*

[3]*School of Physics, Raymond and Beverly Sackler Faculty of Exact Sciences, Tel Aviv University, 69978 Ramat Aviv, Israel*

[4]*Department of Physics, Simon Fraser University, Burnaby, British Columbia, Canada V5A IS6*

[5]*Department of Physics, University of Western Ontario, London Ontario, Canada N6A 3K7*

[6]*Los Alamos National Laboratory, Los Alamos, New Mexico 87545*

[7]*Department of Physics, Ohio University, Athens, Ohio 45701*

(Received 13 February 1998)

Double differential cross sections from the ^{120}Sn$(n,p)^{120}$In and ^{181}Ta$(n,p)^{181}$Hf reactions at 298 MeV and the ^{238}U$(n,p)^{238}$Pa reaction at 318 MeV have been measured for excitation energies up to 50 MeV in the residual nucleus. These data, together with the previously published data from the ^{90}Zr$(n,p)^{90}$Y and ^{208}Pb$(n,p)^{208}$Tl reactions at 198 MeV, have been analyzed for spin-isovector resonances of multipolarities less than 7, using the multipole decomposition method. The strengths due to spin-isovector excitations of multipolarity less than 4 have been extracted. The anomalous behavior of the extracted spin-isovector quadrupole strength with target mass number is discussed with reference to the calculations of Leonardi *et al.* The cross section due to quasifree processes was calculated and subtracted from the data. The data after this subtraction were reanalyzed for spin-isovector resonances and the strengths due to multipolarities up to 3 were extracted. The strengths due to spin-isovector dipole and octupole excitations were compared to values calculated, for $1\hbar\omega$ transitions only, using the sum rules of Macfarlane. The behavior with target mass number is well represented by these sum rules. [S0556-2813(98)06706-5]

PACS number(s): 25.40.Kv, 24.30.Cz, 27.60.+i, 27.70.+q

I. INTRODUCTION

Since the advances made in both accelerator and detector technology in the 1970s enabled the collection of charge exchange reaction data at intermediate energies, numerous studies of such reactions have been reported. However, the majority of these studies have concentrated on the Gamow-Teller resonance. Most of the published data from such reactions have been obtained using targets from the lower mass region of the periodic table, and the cross section induced by these reactions on light to medium mass nuclei is dominated by this resonance. The large neutron excess in heavier elements suppresses this resonance in neutron-induced charge exchange reactions, due to Pauli blocking. Hence the study of such reactions allows one to examine the generally smaller response due to resonances of higher multipolarity.

Recent neutron charge exchange reactions on heavier targets have been reported [1,2] at bombarding energies of 97 and 98 MeV. Unlike the reactions reported here, reactions at such low energies cannot be considered to be simple direct reactions and, therefore, the analyses in those studies are complicated by the necessity of removing the multistep contribution to the cross section. Further, the strength ratio of the spin-flip and isospin-flip components to that of the non-spin-flip and isospin-flip components of the nucleon-nucleon interaction at 100 MeV is only of the order of 2:1, whereas it is in excess of 10:1 in the region of 200–300 MeV [3]. Therefore, the data presented here provide an unambiguous study of the spin-isovector resonances of interest. Finally, the data presented here are of higher resolution than those of other studies, allowing structure to be observed in the measured cross sections.

Numerous theoretical studies of both (n,p) and (p,n) reactions have also been published. These, too, concentrated on the Gamow-Teller resonance, but some also attempted to calculate the cross section due to all processes. An initial comparison between these calculations and the data from (p,n) reactions showed close agreement. However, similar calculations [4–6] compare poorly with the data obtained from the ^{90}Zr$(n,p)^{90}$Y reaction [7,8]. All of these calculations underestimate the cross section beyond 20 MeV excitation, indicating an inadequate treatment of the quasifree cross section, which dominates the response at higher excitation energies. This failing is also seen in the calculations of the inclusive ^{90}Zr$(p,n)^{90}$Nb cross section of Osterfield, Cha, and Speth [9]. The calculations of the inclusive ^{90}Zr$(n,p)^{90}$Y cross section also underestimates the widths of the resonances. Wambach [10] attributes this to the to the inclusion of only collisionless Landau damping, which becomes unimportant for heavy nuclei, rather than collisional damping. Hence the theoretical treatment of (n,p) reactions needs to be improved.

The purpose of this study is to extend the data from (n,p) reactions to the heavy mass region of the periodic table in order that improved theoretical treatments may be tested

*Deceased.

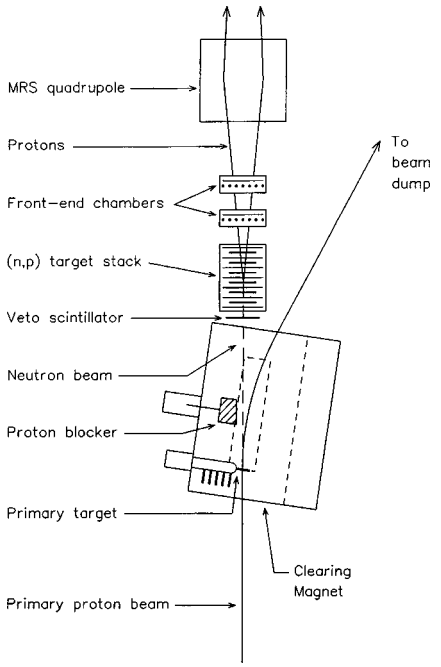

FIG. 1. Schematic diagram of the charge exchange facility at TRIUMF.

TABLE I. Composition of secondary target stacks.

Position	Material	Thickness (mg/cm^2)
a	^{120}Sn	561.7
b	^{120}Sn	560.3
c	^{120}Sn	555.6
d	^{120}Sn	442.8
e	^{120}Sn	438.8
f	CH_2	46.7
a	^{181}Ta	410.99
b	^{181}Ta	407.91
c	^{181}Ta	406.11
d	^{181}Ta	404.95
e	^{181}Ta	406.13
f	CH_2	89.25
a	empty	
b	^{238}U	886.11
c	^{238}U	890.58
d	^{238}U	884.48
e	^{238}U	883.37
f	CH_2	92.39

across the periodic table, especially in the region where the Gamow-Teller resonance is not dominant.

The new data presented here consist of the cross sections induced by (n,p) reactions on ^{120}Sn and ^{181}Ta at a bombarding energy of 298 MeV and ^{238}U at 318 MeV. In order to provide a self-consistent data set, the previously published [7,8] data from (n,p) reactions on ^{90}Zr and ^{208}Pb at 198 MeV were reanalyzed with the new data. ^{181}Ta and ^{238}U were included to provide data from nonspherical nuclei, while ^{181}Ta is also an odd-even nucleus.

II. EXPERIMENTAL DETAILS

The experimental details for the measurements of the ^{90}Zr$(n,p)^{90}$Y and ^{208}Pb$(n,p)^{208}$Tl, reactions are given elsewhere [11]. The new measurements for this work were carried out using the TRIUMF charge exchange facility in the (n,p) mode. The relevant components of the facility are shown in Fig. 1 and are described in more detail in Ref. [12]. Neutrons are produced by the ^{7}Li(p,n) reaction using a proton beam of several hundred nanoamps incident on a target of thickness 220 mg/cm^2. The nominal beam energy for the ^{120}Sn$(n,p)^{120}$In and ^{181}Ta$(n,p)^{181}$Hf reactions was 300 MeV, while that for the ^{238}U$(n,p)^{238}$Pa was 320 MeV. The resulting neutron beams were approximately 2 MeV lower in energy than the proton beam due to the Q value of the neutron-producing reaction.

The protons from the (n,p) reactions on the targets of interest were passed through two sets of drift chambers which provided a measurement of position and direction for each proton as it entered the medium resolution spectrometer (MRS). After momentum analysis in the MRS, the protons were detected in series of drift chambers at the focal plane of the spectrometer. For a given magnetic field setting of the MRS, protons were detected over an energy range corresponding to approximately 50 MeV excitation in the residual nucleus. The initial neutron beam had a resolution of approximately 1.3 MeV, while energy losses in the targets resulted in an increase in the overall resolution to about 1.7 MeV.

The secondary target, detailed in Ref. [13], consisted of up to six layers of target material, each mounted between wire chamber planes, which allowed identification of the target layer from which each proton originated. This identification allows the measured proton energy to be corrected for energy losses in the subsequent target layers. The last target layer in the stack was of polyethylene (CH_2), and the cross section for production of protons from the ^{1}H$(n,p)n$ reaction on the hydrogen in this target was used to normalize the reaction cross section. The details of each stack of targets are given in Table I.

The targets were mounted on a wheel which carried two other target stacks. One of the other stacks consisted of five empty frames before a single CH_2 target, which provided information on experimental background. The third stack consisted of six polyethylene targets and provided information on the relative neutron flux and detector efficiency as a function of target position.

The detection efficiency of the MRS as a function of proton momentum was determined by varying the magnetic field such that the proton groups from the stack containing six CH_2 targets traversed the focal plane. This measurement also provided the momentum and energy calibrations for the spectrometer.

Since the angular acceptance of the spectrometer is approximately 4°, while the difference between the angles at which the spectrometer was set was approximately 3°, there is a large overlap in proton scattering angles obtained. As the scattering angle of each proton is calculated from its trajectory through the detector system, the data may be regrouped into smaller angular ranges than the spectrometer angles provide. The data were regrouped into ranges approximately 2°

TABLE II. Mean laboratory scattering angle for the targets shown.

^{120}Sn		^{181}Ta		^{238}U	
Angle $\langle\theta\rangle$ (deg)	Error $\langle\theta\rangle^2-\langle\theta^2\rangle$ (deg)	Angle $\langle\theta\rangle$ (deg)	Error $\langle\theta\rangle^2-\langle\theta^2\rangle$ (deg)	Angle $\langle\theta\rangle$ (deg)	Error $\langle\theta\rangle^2-\langle\theta^2\rangle$ (deg)
1.33	0.42	1.24	0.36	1.64	0.41
2.90	0.57	2.82	0.62	2.91	0.31
5.02	0.58	5.05	0.64	4.66	0.62
7.07	0.53	6.99	0.47	7.01	0.60
9.45	0.90	9.04	0.60	9.52	0.94
12.51	0.76	11.50	0.95	12.65	0.81
15.89	1.37	13.69	0.29	16.03	1.25

wide, such that there were approximately 10^4 events in each spectrum. The mean scattering angles derived are shown in Table II. These scattering angles may be contrasted with the angles at which the spectrometer was set: 0°, 2.5°, 5°, 8°, 12°, and 16° for ^{120}Sn; 0°, 2.5°, 5°, 8°, and 12° for ^{181}Ta; and 0°, 2.5°, 5°, 8°, 11°, and 16° for ^{238}U.

After corrections for the various detector efficiencies and variation of neutron flux and energy loss for each target layer, the data are then corrected for the experimental background. This background arises from protons which originate from the gas in, and the mylar entrance windows to, the multiwire proportional counters between the targets. The spectra used for this correction are obtained from the target stack containing empty frames and must be corrected for the energy losses and straggling which occur for protons produced from the targets of interest.

The neutron beam produced by the ^{7}Li(p,n) reaction is not truly monoenergetic, but consists of a sharp peak followed by a long tail in energy which has an intensity per MeV of about 1% of that in the peak. The spectra are corrected to remove the effects of this tail by an iterative process, which results in negligible correction at low excitation energies, but results in a correction of about 30% at 30 MeV.

The resulting spectra are then converted to absolute cross section using the yield from the ^{1}H$(n,p)n$ reaction in the polyethylene target and the cross section from this reaction calculated from measured phase shifts [14], at each laboratory scattering angle. This correction is detailed in Ref. [11].

During the calibration from detector plane position to excitation energy in the daughter nucleus, the energy increment for the data is chosen. This choice is arbitrary, and in this case 1.5 MeV increments were chosen as this is approximately the energy resolution of the experiment.

III. DATA ANALYSIS AND RESULTS

The resulting spectra show very little structure and must, in the absence of theoretical predictions, be analyzed using the multipole decomposition method [15]. This method assumes that the measured angular distributions may be adequately described as an incoherent sum of cross sections with various spin and parity transfers:

$$\frac{d^2\sigma}{d\Omega dE_{\rm expt}}=\sum_{\Delta J^\pi} C_{\Delta J^\pi}\frac{d^2\sigma}{d\Omega dE}(\Delta J^\pi).$$

In principle, the sum should run over all allowed spin and parity transfers consistent with the properties of the initial and final states, with the coefficients $C_{\Delta J^\pi}$ determined by fitting the data. However, most of the data were measured at only seven angles, so that a maximum of six terms only may be reliably fitted to the data.

For a given angular momentum transfer ΔL, total angular momentum transfers $\Delta J=\Delta L$, $\Delta L\pm 1$ are possible. Previous studies [16,11] have shown that shapes of the appropriate angular distributions were sensitive mainly to the value of ΔL, rather than ΔJ, and that a suitable shape for a given ΔL could be obtained using an incoherent sum of the shapes from the three ΔJ values.

A. DWIA calculations

Distorted wave impulse approximation (DWIA) differential cross sections were calculated using the program DW81 [17], which sums the contributions from the various particle-hole configurations coherently. The transition amplitudes were calculated [18] using simple harmonic oscillator wave functions. The configuration space was restricted to $\pm 2\hbar\omega$ from the proton and neutron Fermi surfaces. Only the strongest few transitions, comprising greater than 80% of the total strength, for each ΔJ^π, were considered in order to limit the computational difficulty of these calculations. The amplitudes were normalized such that the sum of the squares was unity, and so the oscillator length does not appear.

The optical model potentials (OMP's) used in this work were calculated using the theory developed by Hüfner and Mahaux [19] and refined by von Geramb *et al.* [20]. This theory associates the OMP with the self-energy of a nucleon propagating through nuclear matter. The code OPMOD [21] was used to generate pointwise potentials using the nuclear charge distributions given by De Vries *et al.* [22] and the Paris nucleon-nucleon potential [23].

DWIA calculations were made for each ΔJ^π value up to $\Delta L\leqslant 3$ and $\Delta J=\Delta L$ for $\Delta L=4,5,6$ at excitation energies of from 0 to 30 MeV, in 5-MeV increments, in the residual nucleus. As mentioned earlier, each of the appropriate ΔJ^π angular distributions, for a given $\Delta L\leqslant 3$ at each excitation energy, was summed incoherently to produce the shapes used in fitting the data. Further, a shape representing contributions from higher multipolarities was constructed from the incoherent sum of the $\Delta L=4$, 5, and 6 angular distributions.

Raywood [7] has shown that strength due to spin-isovector monopole (SIVM) and Gamow-Teller (GT) excitations in a heavy nucleus, where both can contribute significantly, cannot be extracted unambiguously via a multipole decomposition analysis. This is because the shape of the SIVM angular distribution can be simulated by the incoherent sum of the GT distribution with that of a higher multipolarity. Since very little Gamow-Teller strength is expected in (n,p) reactions on heavy nuclei, due to the large neutron excess, only angular distributions from SIVM excitations were used in this analysis. Hence all $\Delta L=0$ strength is attributed only to SIVM excitations.

B. Multipole decomposition

The multipole decomposition method relies on the assumptions that the angular distribution of each multipolarity

is distinguished by the angle at which it peaks and that this angle is primarily determined by the orbital angular momentum transfer of the transition. It is further assumed that there is no interference between the multipole transitions.

Thus the angular distribution at a given excitation energy is analyzed on the basis that it consists of an incoherent combination of the angular distributions of the possible multipoles. This can be written as

$$\left(\frac{d\sigma}{d\Omega}\right)_{\text{expt}} = \sum_L a_L \left(\frac{d\sigma}{d\Omega}\right)_L ,$$

where L is the orbital angular momentum transfer associated with each of the resonances, a_L is the relative strength of the individual multipoles and depends only on excitation energy, and the $(d\sigma/d\Omega)_L$ are the theoretical DWIA angular distributions for each multipolarity. Therefore, the analysis consisted of finding the various a_L values over the range of excitation energies obtained, for each of the experimental targets.

In order to produce a self-consistent data set, both the ^{90}Zr$(n,p)^{90}$Y and ^{208}Pb$(n,p)^{208}$Tl data at 198 MeV, of Raywood [7] were reanalyzed, together with the new data presented here. The data were only analyzed to 30 MeV excitation in the daughter nucleus in order to easily compare the results with those obtained after the quasifree cross section had been subtracted (see below). The results of this analysis are shown in Fig. 2–6. The errors associated with this analysis are discussed in a separate section later.

However, it should be noted that these figures are reconstructed from the analyses of the angular distributions at each energy increment. These angular distributions were fitted very well by the incoherent combination of theoretical DWIA angular distributions of multipolarity less than $\Delta L = 7$. The apparently poor fits at the largest scattering angle in ^{90}Zr, ^{208}Pb, and ^{238}U are due to the truncation of the ΔL values used in the fitting process. The apparently poor fit to the ^{181}Ta data at 9° is due to the data lying between the angles at which $\Delta L = 3$ and the $\Delta L > 3$ distributions peak (7° and 11°, respectively).

The integrated cross sections for all of the multipole components present in each of the targets are summarized in Table III. These were derived by summing the cross section of each component present in each excitation energy bin. The resulting angular distributions of energy integrated cross section were then fitted with the angular distribution for each component to produce a normalization factor for the total cross section given by DWBA81.

The results from the reanalysis of Raywood's data are very consistent with his analysis. Significant strength from all multipolarities less than 4 was found across the mass range analyzed here. Strength due to multipolarities greater than 3 was found in all of the data, but was not resolved into particular multipolarities.

These results are also qualitatively similar to those of Condé *et al.* [1] and Ringbom *et al.* [2], although more structure can be seen in the results presented here.

Most of the spin-multipole cross section found was distributed fairly evenly up to 20 MeV, with little evidence for general concentrations of strength. However, there is strong evidence for giant spin-dipole resonances at low excitation energies in all of the data.

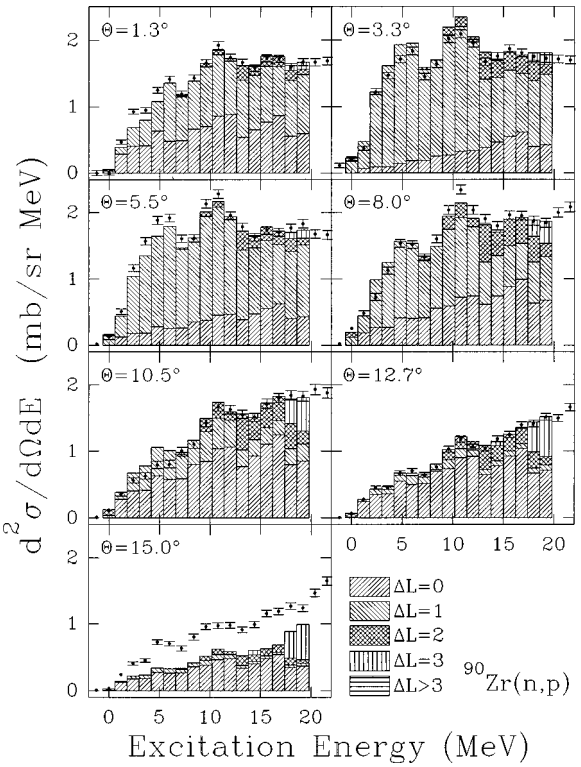

FIG. 2. Results of the multipole decomposition of the data from the ^{90}Zr$(n,p)^{90}$Y reaction. The data are represented by the vertical error bars, and the contribution deduced for each multipolarity is shown as the filled histogram bars. The strength deduced for spin-isovector monopole reactions at each excitation energy bin is shown as a diagonal fill sloping left to right. The contribution due to spin-isovector dipole excitations is shown as the right to left diagonal fill. The spin-isovector quadrupole contribution is shown as hatched bars, while that due to spin-isovector octupole excitations is shown as the vertically filled bars. The contribution deduced for excitations of multipolarity greater than 3 is shown by the horizontally filled bars. Note that the data at laboratory angles of 17.3°, 19.4°, and 22.3° were also analyzed, but the results are not shown here.

One feature of the cross sections extracted in this analysis is that the spin-isovector quadrupole (SIVQ) ($\Delta L = 2$) cross section varies considerably with the targets studied. This behavior is most apparent when one compares the cross section extracted from the two deformed nuclei studied. In the case of ^{181}Ta, the SIVQ excitations dominate the spectra, while there is negligible cross section of this multipolarity evident in ^{238}U. Further, a negligible SIVQ was extracted from the analysis of ^{90}Zr, while both ^{120}Sn and ^{208}Pb show significant SIVQ contributions.

Other analyses have also found anomalous SIVQ strength. The analysis of El-Kateb *et al.* [24] found that SIVQ excitations dominated the ^{55}Mn(n,p) reaction, while similar reactions on ^{56}Fe and ^{58}Ni showed very little SIVQ strength. Vetterli *et al.* [25] also found significant SIVQ strength in the ^{54}Fe(n,p) reaction, although this also includes contributions from higher multipolarities. Such a large variation in strength within such a small region of the periodic table makes generalization of SIVQ behavior across the periodic table very difficult.

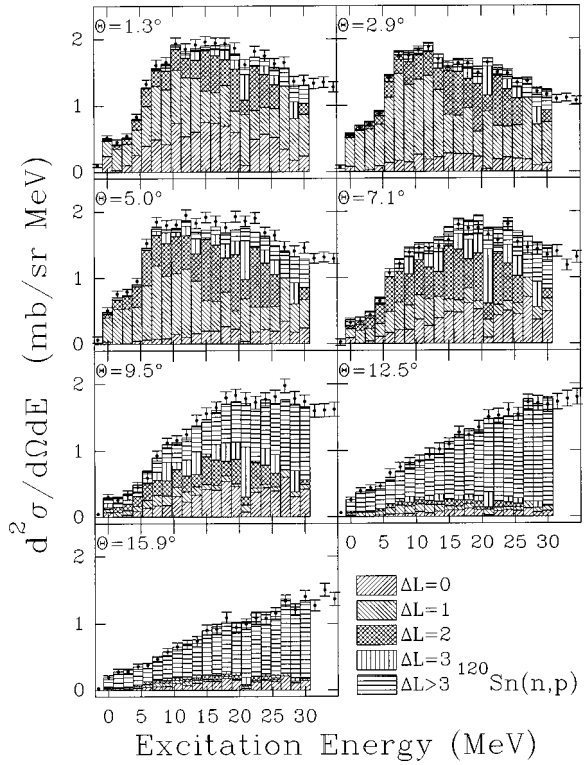

FIG. 3. Results of the multipole decomposition of the data from the ^{120}Sn$(n,p)^{120}$In reaction. See Fig. 2 for an explanation of the symbols used.

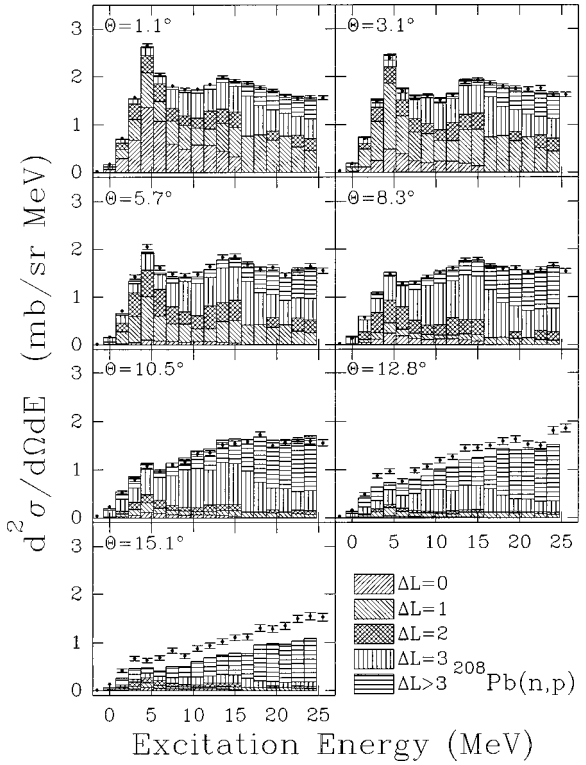

FIG. 5. Results of the multipole decomposition of the data from the ^{208}Pb$(n,p)^{208}$Tl reaction. See Fig. 2 for an explanation of the symbols used. Note that the data at laboratory angles of 17.4°, 19.9°, and 22.6° were also analyzed, but the results are not shown here.

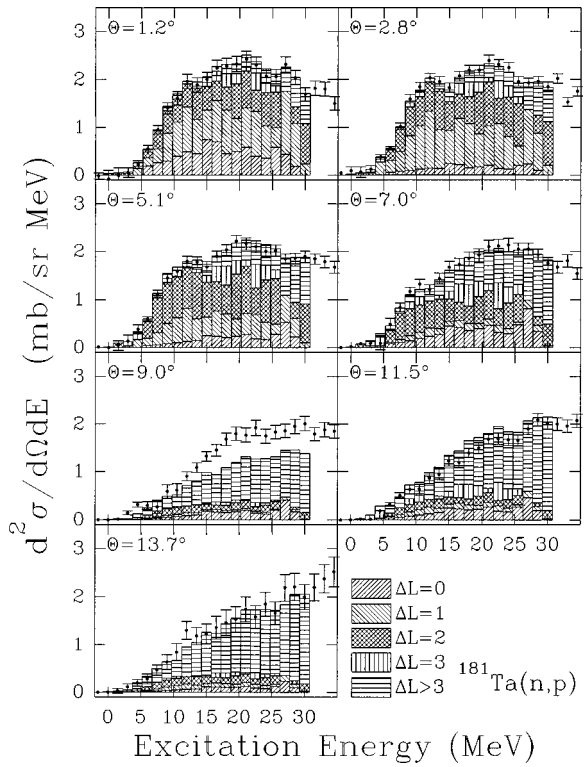

FIG. 4. Results of the multipole decomposition of the data from the ^{181}Ta$(n,p)^{181}$Hf reaction. See Fig. 2 for an explanation of the symbols used.

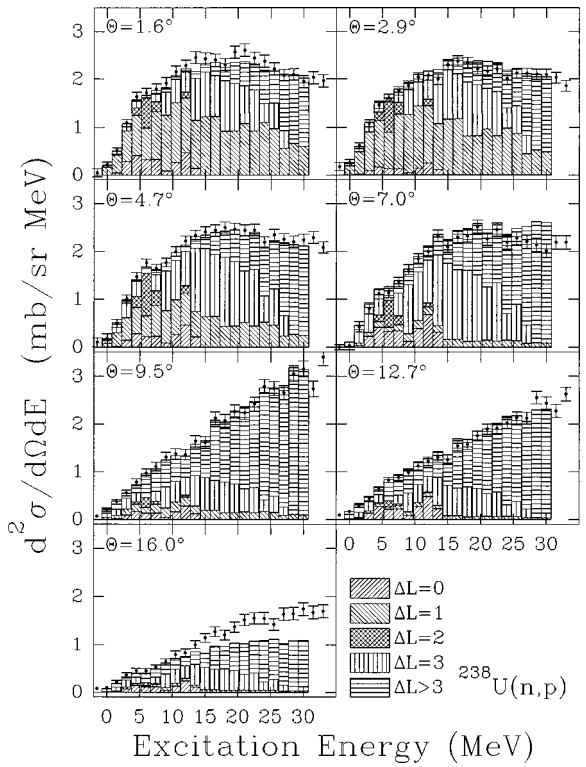

FIG. 6. Results of the multipole decomposition of the data from the ^{238}U$(n,p)^{238}$Pa reaction. See Fig. 2 for an explanation of the symbols used.

TABLE III. Integrated cross sections for each of the multipole contributions, obtained by multiplying the DWIA total cross section for an appropriate ΔJ^{π} by a normalization factor.

	Integrated cross section (mb)			
Target	$\Delta L=0$	$\Delta L=1$	$\Delta L=2$	$\Delta L=3$
^{90}Zr	2.9	0.47	0.11	0.20
^{120}Sn	1.8	1.4	1.4	0.87
^{181}Ta	1.2	0.92	1.8	0.66
^{208}Pb	1.7	1.4	1.1	3.9
^{238}U	1.0	1.5	0.21	5.1

Leonardi *et al.* [26] have investigated the fact that the SIVQ strength present in the ^{90}Zr(p,n) reaction is much smaller than that predicted by random phase approximation calculations. Leonardi *et al.* found that the presence of a low-lying $0\hbar\omega$ quadrupole state in ^{90}Nb together with the introduction of nonlocal components to the interaction can suppress SIVQ strength in this reaction. Leonardi *et al.* also found that the SIVQ strength induced by neutron charge exchange reactions is enhanced by this mechanism. Such a mechanism may explain the anomalous SIVQ strength in the other targets. If the presence of the low-lying rotational state is taken to mean collectivity in the (p,n) daughter, then this mechanism may be generalized to state that strong SIVQ excitations will be found in (n,p) reactions on targets with collectivity in the (p,n) daughters.

Applying this generalization to the targets studied here, neither ^{90}Nb nor ^{238}Np shows collectivity through rotational level structure or coherent particle-hole wave functions, while ^{120}Sb and ^{181}W are strongly collective nuclei and ^{208}Bi shows some signs of collectivity.

C. Quasifree cross section

While the cross section for intermediate-energy scattering is dominated by giant resonances at low excitation energies, the quasifree interaction dominates the high-excitation-energy region. These excitations involve energy transfers of $2\hbar\omega$ or greater. In the intermediate-excitation-energy region, the cross section due to quasifree scattering underlies the structure due to $1\hbar\omega$ giant resonances.

Several authors [27,11,28] have used empirical functions fitted to the data to account for this cross section. This approach is not applicable to most of the spectra analyzed here due to the absence of sharp features. Rather, the quasifree component is calculated from a purely theoretical basis.

Developed by Esbensen and Bertsch [29] and Smith and Wambach [30], this theory is based on the nucleon-nucleus cross section having the form

$$\frac{d^2\sigma}{d\Omega dE}=N_{\rm eff}\sum_{T,S}\ \frac{k'}{k}\ {\rm tr}\{f^{*}_{TS}(\vec{q})f_{TS}(\vec{q})\}S_{TS}(q,\omega).$$

Here the sum is over the spin and isospin transferred to the nucleus. S_{TS} is the nuclear response function in the spin and isospin channel, and f_{TS} is the spin and isospin piece of the free NN amplitude. The trace is over both projectile and target nucleon spins, normalized such that ${\rm tr}(\sigma_i)=0$ and ${\rm tr}(1)=1$. $N_{\rm eff}$, is the effective number of nucleons seen by the projectile and is determined from the in-medium total NN cross section σ_{NN}. While σ_{NN} is calculated [38], the calculated cross section is subsequently normalized to the data.

In order to easily incorporate the surface-peaked nature of the probe-nucleus interaction, Esbensen and Bertsch developed the slab model, in which the nucleus is modeled as a semi-infinite slab of nuclear matter. The probing field, given by

$$\theta_{\vec{q}}(\vec{r})=e^{i\vec{q}\cdot\vec{r}}e^{-\sigma T(b)/2},$$

confines the scattering to the surface. This field is generated using only the absorptive part of the optical potential.

Smith and Wambach [31] have extended this theory to include two-particle–two-hole (2p-2h) excitations and have found that this improves the agreement with the data. Unfortunately, the inclusion of such multistep processes greatly increases the computational complexity of the calculation and was not undertaken here. However, these authors report [30] that ''The two step cross section . . . produces a flat [*ie* smooth] background which steadily rises from 0 to about 1 mb/sr/MeV at 60 MeV excitation energy.'' Multistep processes were, therefore, included empirically by adding a quadratic, which peaked beyond the maximum measured excitation energy, to the calculated cross section.

Since the theoretical calculations were performed under the assumption of the slab model, the calculated 1p-1h quasifree cross sections do not incorporate the binding energy of the struck nucleon. Therefore, these calculations were shifted in excitation energy by the binding energy of the proton in the daughter nucleus. Note, however, that this shift in energy introduces uncertainty regarding the possible double counting of the $1\hbar\omega$ quasifree excitations. It can, therefore, be regarded as no more than a phenomenological way of treating the quasifree cross section. The calculated spectra were then interpolated to the same excitation energy bins as the data.

A preliminary comparison between the calculated quasifree cross sections and the data suggested that all of the cross section above 25 MeV in excitation was due to quasifree processes, because of the similarity in shape. Therefore, the data above 25 MeV were fitted with a linear combination of the calculated 1p-1h quasifree cross section and an empirical function, the latter representing the multistep contributions to the quasifree cross section. This can be represented as

$$\left(\frac{d^2\sigma}{d\Omega dE}\right)_{\rm expt}=N_1\left(\frac{d^2\sigma}{d\Omega dE}\right)_{\rm calc}+N_2[C^2-(C+B-X)^2],$$

$$X\geqslant 25\ \ {\rm MeV},$$

where N_1 and N_2 are normalization parameters, X is the excitation energy, B is the proton separation energy, and C is the maximum measured excitation energy. The quasifree cross section was set to zero for excitation energies less than the proton separation energy.

This procedure has the advantages that (i) there are only two independent parameters in the fitting procedure and (ii) the shape of the quasifree cross section under the data is

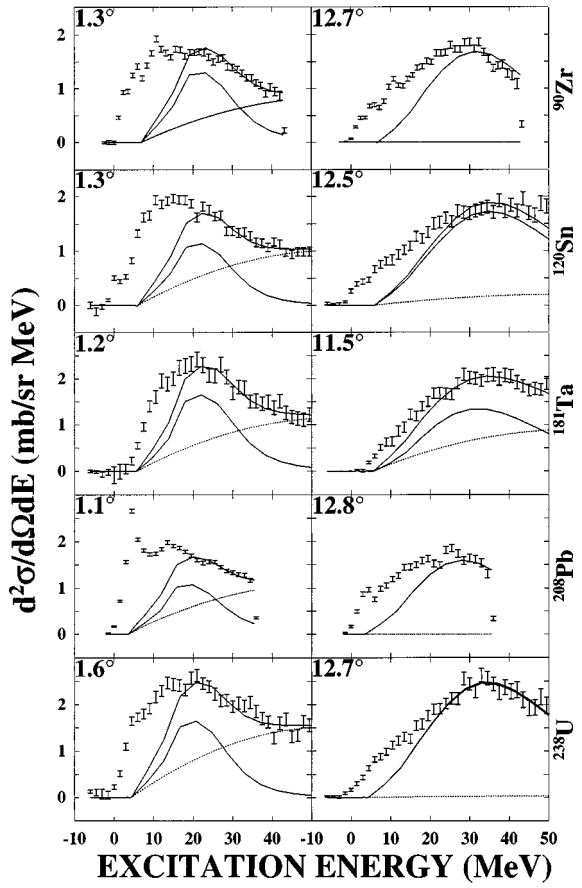

FIG. 7. Comparison between the fitted quasifree cross section and the data at laboratory angles of approximately 1° and 12°. The data are represented by the error bars, while the overall fit is shown as the solid lines. The relative contributions of the calculated and empirical components are shown as the dashed and dotted lines, respectively. Note that, in most cases, the calculated cross section and the total fit are nearly identical at 12°.

independent of any assumed giant resonance structure. The results of these fits at laboratory angles of about 1° and 12° are shown in Fig. 7. Here the overall fit is represented by the solid lines, the fitted cross sections of the single-step processes are shown as the dashed lines, and the empirical functions are shown as dotted lines. The overall fits show excellent agreement with the data in the region above 25 MeV in excitation, where the cross section at small scattering angles is dominated by the empirically fitted cross section. The agreement between the data and the fit at these energies suggests that the assumption made for the shape of the multistep contributions to the quasifree cross section was reasonable.

The excitation region between 19 and 25 MeV, which was not included in the fitting procedure, also shows excellent agreement between the fit and the data. At small angles, the quasifree cross sections peak at about 20 MeV excitation. The agreement between the data and the fit in the region between 19 and 25 MeV justifies shifting the calculated cross sections as described earlier.

The only conclusion that can be drawn from these results is that the formalism of Smith [32] does produce a good representation of the shape of the quasifree cross section in nucleon-nucleus scattering.

D. Multipole decomposition without the quasifree cross section

Consider now the components of the spectra which do not fall under the heading of ''quasifree scattering.'' From the discussion in the previous section, this data set is confined to excitation energies below 19 MeV and, as noted, is not accounted for by the quasifree scattering calculations. That is, we now refer to transitions in which the struck nucleon cannot be considered as free. In other words, we are now referring to transitions which leave the neutron *within* the single-particle well which now represents the final nucleus. This is true whether we are referring to the incident neutron captured into the nuclear potential or the neutron of the $p \rightarrow n$ transition within the target nucleus. Such states are just the single-particle states which give rise to the giant resonance phenomenon in nuclear structure calculations where the residual interaction is taken into account.

Thus, to some approximation, subtracting the quasifree component from the total data set will give a series of spectra which are the sums of the giant resonances of varying multipolarity. In terms of the nuclear structure of the residual nuclei, the spectra remaining after this subtraction are sums of 1p-1h $1\hbar\omega$ transitions of multipolarity 0–3. To put this another way, the subtraction of the quasifree cross section, as described, is in fact a phenomenological way of obtaining the contributions of the $1\hbar\omega$ giant resonances to the cross sections. It must be emphasized, however, that the result of this subtraction cannot be regarded as giving more than a rough estimate of these giant resonances. The fact that the contributions of the various L values are determined again by a multipole decomposition process merely adds weight to this statement.

The data resulting from the subtraction of the quasifree component were analyzed in the same manner as described earlier. The results of this analysis are shown in Fig. 8. The total cross sections of the various multipoles (up to $\Delta L = 3$) found in each of the targets are summarized in Table IV. We now wish to compare these results, for the $\Delta L = 1$ and 3 transitions, with calculations using the Macfarlane sum rules [33] for charge exchange reactions.

E. Comparison with sum rules

Macfarlane [33] has developed sum rules obtained from the energy moments of multipole strength functions. These sum rules may be compared with the total strength extracted from data such as those described in the previous section. Macfarlane began with the strength function

$$\Gamma(E) = \sum_f \delta(E - E_f) |\langle f | M_j^L | O \rangle|^2,$$

where O is the ground state, f labels the eigenstates of the residual nucleus, E is the energy, and M_j^L is a multipole operator of total angular momentum j and multipolarity L. For isovector excitations, the operator is

$$M_j^{\pm L} = \sum_{i=1}^{A} m_j^L(i) t^{\pm}(i),$$

where $t^{\pm}$ is the isospin-raising or lowering operator.

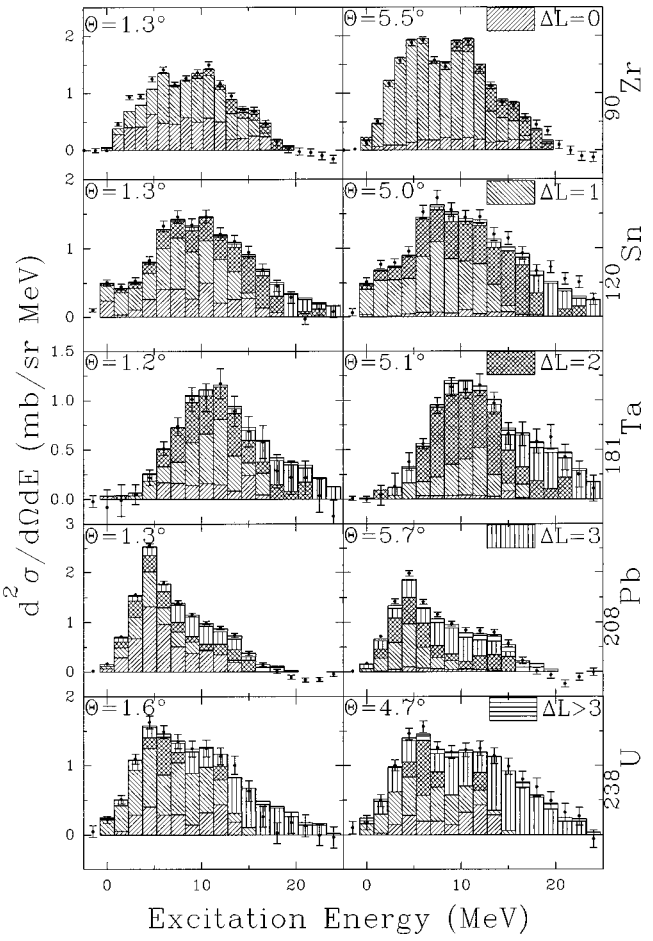

FIG. 8. Results of the multipole decomposition of the data from the (n,p) reactions on each of the targets (as indicated) after subtraction of the quasifree cross section, at laboratory angles of approximately 1° and 5°. The data are represented by the vertical error bars, and the contribution deduced for each multipolarity is shown as the filled histogram bars. The strength deduced for spin-isovector monopole reactions at each excitation energy bin is shown as a diagonal fill sloping left to right. The contribution due to spin-isovector dipole excitations is shown as the right to left diagonal fill. The spin-isovector quadrupole contribution is shown as hatched bars, while that due to spin-isovector octupole excitations is shown as the vertically filled bars. The contribution deduced for excitations of multipolarity greater than 3 is shown by the horizontally filled bars.

In order to obtain an expression for the total strength of an excitation, in which the ground state structure only enters through orbit occupation numbers, Macfarlane used two assumptions: first, that the angular momenta of the protons and neutrons separately couple to zero total angular momentum in the target ground state and, second, that single-particle (and the corresponding single-hole) wave functions with the same orbital and total angular momentum numbers, but different principal quantum numbers, are orthogonal. The second assumption is exact in the mean-field limit, while the first assumption should only be good for doubly closed shell nuclei.

In the case of (n,p) reactions, the resulting sum rule for the total strength of a particular multipole operator can then be expressed in terms of the reduced matrix element of the operator and the fractional neutron and proton occupation numbers n_ρ^ν and n_ρ^π. Within a spherical basis, the sum rule for a particular multipolarity L is given by

$$S_L=\frac{1}{(2L+1)}\sum_{\rho\rho'}|\langle\rho'\|r^L[\mathbf{Y}_L\times\boldsymbol{\sigma}]_j\|\rho\rangle|^2 n_\rho^\pi(1-n_{\rho'}^\nu),$$

$$\rho=(nlj),\quad L\geqslant 0.$$

In order to compare these sum rules with the experimental data referred to in the previous section, and summarized in Table IV, calculations were made only of the strength of the $1\hbar\omega$ excitation for the dipole and octupole excitations ($\Delta L=1$ and 3) in the targets used in this work. The reduced matrix element above becomes

$$\langle\rho'\|r^\lambda[\mathbf{Y}^\lambda\times\boldsymbol{\sigma}]_j\|\rho\rangle=\frac{1}{2}\sqrt{\frac{6}{\pi}}\hat{j}'\hat{J}\hat{\lambda}\hat{l}\hat{j}C^{l'0}_{l0\lambda0}\begin{Bmatrix} l' & \frac{1}{2} & j' \\ l & \frac{1}{2} & j \\ \lambda & 1 & J\end{Bmatrix}\times\int_0^\infty\mathcal{R}_{n'l'}(r)\mathcal{R}_{nl}(r)r^{\lambda+2}dr.$$

Using the relation

$$\begin{pmatrix} l & \lambda & l' \\ 0 & 0 & 0\end{pmatrix}=\frac{(-1)^{l-\lambda}C^{l'0}_{l0\lambda0}}{\hat{l}'},$$

harmonic oscillator radial wave functions obtained from Lawson [34], the simplifications for the 9-j symbol given by Brink and Satchler [35] and the ground state occupation probabilities given by Bleuler *et al.* [36], the radial matrix element was evaluated for each of the targets of interest here.

TABLE IV. Integrated cross section for each of the multipole contributions, after subtraction of the quasifree cross section.

Target	Integrated cross section (mb) $\Delta L=0$	$\Delta L=1$	$\Delta L=2$	$\Delta L=3$
^{90}Zr	1.6	0.33	0.13	0.045
^{120}Sn	0.39	0.72	0.93	0.61
^{181}Ta	0.19	0.28	0.75	0.58
^{208}Pb	0.33	0.48	0.70	1.6
^{238}U	1.2	0.46	0.20	2.3

Figure 9 shows the comparison between the results of this calculation and the experimental results given in Table IV. In this comparison, it was assumed that the cross section was proportional to the strength and that the A dependence of the proportionality could be neglected. Since the calculations were not made in absolute units, they were normalized to the data, excluding only those data from the ^{181}Ta$(n,p)^{181}$Hf reaction. Given the limitations of the calculation and the assumption that subtraction of the quasifree cross section from the data leaves only the cross section due to $1\hbar\omega$ transitions only, the agreement is surprisingly good.

It should be noted that, for comparison with the ^{181}Ta data, the sum rules were calculated for ^{182}W. This case gives

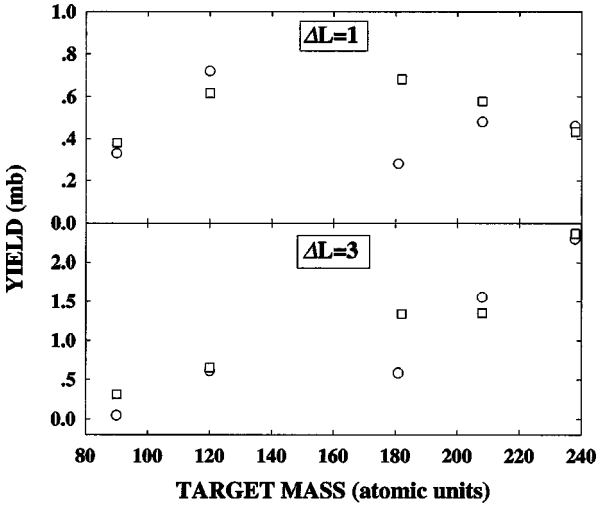

FIG. 9. Comparison between the calculated sum rules (squares) and extracted spin-isovector dipole and octupole strengths, after subtraction of the quasifree cross section (circles).

the worst comparison of all the targets, which is not surprising since ^{182}W has neither a proton nor neutron shell closed, thereby drastically breaking the first assumption in Macfarlane's treatment. Furthermore, ^{181}Ta is a known nonspherical nucleus, and therefore the angular distributions used in the multipole decomposition are more dubious than for the other nuclei. Further, the deformation of this nucleus will spread the strengths to a greater extent than the other nuclei.

The ^{238}U nucleus is generally regarded as nonspherical and quadrupole deformed, because of the presence of rotational bands in its energy level scheme. However, the present results indicate a much larger $\Delta L=3$ component than the $\Delta L=2$ component and raise the question of whether rotational bands could be generated by such an admixture.

F. Uncertainties in the results

1. Angular distribution shapes

As described earlier, the inputs used in calculating the angular distributions were the free nucleon-nucleon force as parametrized by Franey and Love [37], optical model potentials calculated using the method of von Geramb [38], and transition densities of select transitions calculated within a harmonic oscillator basis.

Raywood [7] has found that the use of the nuclear density-dependent form of the two-nucleon t matrix [38] from the Paris potential [23] produces negligible differences in the angular distributions. The effects of using such a t matrix in the calculations for this work were not tested in detail. However, it is expected that the results found by Raywood are general and that any variation would be insignificant.

The optical model potential strongly influences the cross section at small angles for transitions which transfer greater than zero angular momentum. The absence of elastic scattering data at the bombarding energies used in this work necessitated the use of theoretical calculations of the optical model potentials. While it is felt that the method of von Geramb produces the best results possible, alternative potentials could strongly influence the amount of $\Delta L=0$ strength found.

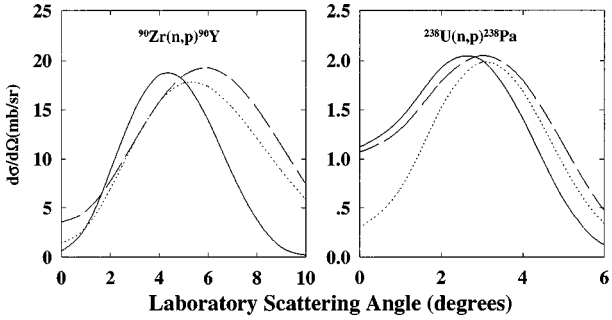

FIG. 10. Angular distributions used to model the spin-isovector giant resonances in ^{90}Zr (left) and ^{238}U (right) at an excitation energy of 0 MeV. The $J^\pi=0^-$ shape is represented by the solid line, and the dashed line represents the $J^\pi=1^-$ shape, while the $J^\pi=2^-$ shape is shown as the dotted line.

The transitions used in calculating the various angular distributions were selected such that greater than 80% of the total transition strength was exhausted. However, the transition densities were calculated within a simple harmonic oscillator basis. The use of a more realistic basis could influence the actual transition amplitudes and, hence, influence the actual transitions used. Alford *et al.* [16] has shown that the choice of transition used to model the giant resonance can influence the angle at which the angular distribution peaks and, hence, the multipole strength deduced. However, Alford *et al.* used only a single transition, while this work uses a coherent sum of several 1p-1h transitions in each calculation. Thus the small differences in the cross section due to each particular transition choice are not resolved in this work.

Figure 10 shows the individual J^π shapes for $\Delta L=1$ transitions in ^{90}Zr and ^{238}U at an excitation energy of 0 MeV. In each case, the shape for $J^\pi=0^-$ peaks at a smaller angle than the other two shapes. Comparison between the two targets shows that the difference between the shapes decreases with increasing atomic number. However, it should be noted that the shapes have been normalized to a standard peak value in the diagram, whereas they were summed to obtain the overall shape without normalization. As the $J^\pi=0^-$ peak cross section is approximately 60% that of the $J^\pi=1^-$ shape, the overall shape used in the multipole decompositions is most like that of the $J^\pi=1^-$ shape. This effect is also seen in quadrupole and octupole shapes.

The effect of summing the various J^π shapes is to produce overall ΔL shapes which are broader than the individual components and peaked close to the $\Delta J=\Delta L$ shape. However, the limited angular resolution of the data precluded using individual J^π shapes in the multipole decomposition.

The shapes used for the various multipole resonances in the multipole decomposition of ^{90}Zr and ^{238}U at 0 and 20 MeV are shown in Fig. 11. As can be seen, at low excitation energies the various shapes are well differentiated. However, as excitation energy increases, the differences in shape become less well defined due to distortion of the incoming and outgoing waves. In each case, the shape used to represent monopole excitations becomes more like that used to repre-

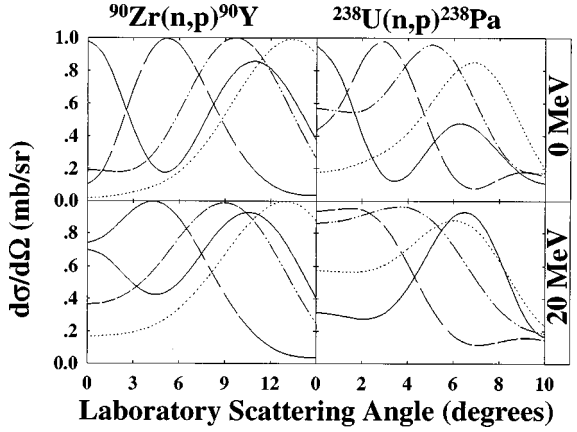

FIG. 11. Multipole resonance shapes used in the multipole decompositions of ^{90}Zr (left) and ^{238}U (right) at excitation energies of 0 MeV (top) and 20 MeV (bottom). The monopole shape is shown as the solid line, the dipole as the dashed line, the quadrupole as the dash-double-dotted line, and the octupole as the dotted line.

sent higher multipolarities, as the peak at 0° decreases, while the secondary peak increases slightly. The shapes used for higher multipolarities also become less well differentiated due to the increasing cross section at small angles.

The effect of changes of angular distribution shape with excitation energy is that the multipole decomposition method used is less reliable in separating the various multipole contributions at high excitation energies. The results at energies below 10 MeV should be reliably given by this method, while the errors induced by this behavior are impossible to quantify in the absence of more realistic angular distributions. The contributions of both monopole and dipole transitions in each target are predominantly in the region below 10 MeV, and therefore these results will be less affected by this behavior than the quadrupole and octupole strengths derived from the multipole decompositions presented here.

2. Quasifree cross section

The results presented earlier are strongly influenced by the choice of quasifree cross section used, especially the low-excitation-energy shape. The calculated cross section used here, like all calculations of the continuum cross section, do not treat Pauli blocking at all. This could have significant effects at low excitation energies and the small angles used. However, the shapes used here are very similar to those used by other authors; therefore, in the absence of more realistic calculations, the results presented here are comparable.

The results presented here are integrated over excitation energy up to approximately 25 MeV. The exact excitation energy to which the strength was summed was primarily determined by that energy beyond which all of the cross section was attributed to quasifree processes. While the contribution from multipole resonances to the cross section in this region is expected to be small, this analysis may underestimate the total strength by neglecting any such contribution.

3. Summary

Various factors contribute in a nonquantifiable manner to systematic uncertainties in the results presented here. The factors which would be expected to most influence the results are the actual shapes used in the decomposition process and the low-excitation-energy profile of the continuum cross section.

Given the limitations of the shapes used in the decomposition process itself, those cases where only a small amount of strength, primarily quadrupole and octupole strength, was found may be in error by as much as a factor of 2. However, the error associated with the amount of dipole strength found may be as low as 20%, given the large contribution it makes to the overall spectrum and the small ambiguity it presents to the decomposition process.

Special mention needs to be made of the ambiguity in separating the $\Delta L=0$ strength into monopole and Gamow-Teller contributions. Throughout this analysis, all of the $\Delta L=0$ strength has been assigned to monopole transitions. However, the amount of Gamow-Teller strength in this mass region is expected to be small, and therefore the error associated with this simplification should be small. Furthermore, Raywood [7] has shown that the strength associated with higher multipolarities does not depend significantly on whether Gamow-Teller or monopole transitions are used for the $\Delta L=0$ component.

IV. DISCUSSION AND CONCLUSION

This work presents the first self-consistent analysis of data from neutron-induced charge exchange reactions on heavy targets, at intermediate energies, for evidence of spin-isovector giant resonances. While many authors have presented analyses of other such data, they have concentrated on Gamow-Teller resonances and have, therefore, only considered reactions on light to medium mass targets in their studies. The heavy targets used for this work preclude strong Gamow-Teller excitations due to Pauli blocking in nuclei with large neutron excesses. The absence of strong Gamow-Teller resonances in the data used here facilitates the search for resonances of higher multipolarity, such as spin-isovector dipole and quadrupole resonances, as well as the spin-isovector monopole resonance. The targets studied here span the mass number range from 90 to 238 and include two nonspherical nuclei and an odd-even nucleus.

The presence of strong Gamow-Teller resonances has also masked deficiencies in previous theoretical studies of intermediate-energy charge exchange reactions. While microscopic calculations of (p,n) spectra reproduce the Gamow-Teller resonances quite well, they fail to adequately model the spectra at higher excitation energies. Microscopic calculations of (n,p) spectra also fail due to systematic underestimation of the widths of other spin-isovector giant resonances. The failures of these calculations are due to effects common to both (n,p) and (p,n) reactions, namely, inadequate treatment of the quasifree cross section and exclusion of collisional damping in calculating resonance widths within the random phase approximation (RPA). This study extends the mass range of reactions against which improved microscopic calculations may be tested.

Spin-isovector dipole (SIVD) excitations dominate the spectra for all targets. Analysis of the data from all targets show evidence for compact SIVD resonances at excitation energies between 5 and 15 MeV in the residual nucleus.

All of the reactions studied here show significant strength due to SIVM excitations. It should be noted that all of the strength from $\Delta L=0$ excitations is attributed to monopole resonances, since the contribution from Gamow-Teller resonances is expected to be small. In general, the extracted $\Delta L=0$ strength shows little evidence for compact resonances.

Analysis of most of the data presented here shows little contribution due to SIVQ excitations relative to that of spin-isovector octupole (SIVO) excitations. However, these contributions are about equal in the case of the ^{120}Sn$(n,p)^{120}$In reaction, and the contributions of quadrupole excitations in the ^{181}Ta$(n,p)^{181}$Hf reaction exceed those due to octupole excitations. This result is most noticeable when one compares the data from the two deformed targets studied, namely, ^{181}Ta, where SIVQ strength may exceed SIVO strength by more than 100%, and ^{238}U, in which negligible SIVQ strength was found, but SIVO strength dominates the spectra at larger angles.

Leonardi *et al.* [26] have proposed a mechanism whereby the existence of a low-lying $0\hbar\omega\ 2^+$ quadrupole state in the (p,n) daughter nucleus, together with the introduction of nonlocal components in the interaction, can produce large amounts of SIVQ strength in (n,p) reactions on the same target. While Leonardi *et al.* only studied this effect in ^{90}Zr, if the mechanism is stated more generally as ''targets with strongly collective (p,n) daughters produce large amounts of SIVQ strength in (n,p) reactions,'' it may explain this behavior.

Strength due to spin-isovector excitations of multipolarity greater than 3 was found in all of the reactions studied here. However, this strength was not resolved into individual multipolarities.

Most of the strength above 15 MeV excitation in the residual nucleus may be attributed to quasifree reactions. These interactions were considered to be excitations of one or more nucleons into the continuum or spin-isovector excitations of several $\hbar\omega$. The cross section due to such reactions underlies that due to the spin-isovector excitations of interest here and was subtracted from the data for some of this analysis. While many authors have used empirical functions to represent this cross section, the absence of distinct features below 15 MeV in the data analyzed here precludes this method.

The quasifree cross section calculated by Smith [39] was used here, although it was found that the addition of a slowly increasing empirical function was needed to fit the data at high excitation energies. This calculation is based on the theory developed by Esbensen and Bertsch [29] and Smith and Wambach [30,31] and assumes a slab model of the nucleus. While the slab model is an improvement over the Fermi gas model of the nucleus, in that it limits the response to the nuclear surface, it fails to account for the binding energy of the struck nucleon in finite nuclei. Pauli blocking is also not treated by this theory, which may result in an overestimation of the cross section at small excitation energies. It should be noted that the calculation used in this analysis considers only single scattering, while Smith and Wambach [31] have shown that inclusion of two-step processes increases the cross section at large excitation energies. The empirical addition used here was proposed as an *ad hoc* method of correcting for this deficiency. However, this addition was not needed at scattering angles greater than 12°, which indicates that it corrected for other deficiencies in the calculation. Nonetheless, the model used for this analysis is very successful in describing the quasifree cross section and has the benefit that it requires only two free parameters to fit the data at each scattering angle.

After subtraction of the quasifree cross section, the data were again analyzed for spin-isovector excitations. The extracted SIVM and SIVD strengths were considerably less than those extracted before the subtraction. The extracted SIVQ and SIVO strengths were not reduced to such extents and, therefore, were effectively enhanced by subtraction of the quasifree cross section.

After subtraction of the quasifree cross section, the extracted SIVD and SIVO strengths follow the trend with mass number predicted by Macfarlane [33] within a factor of 2 at each individual point. This close agreement shows that the calculated cross section adequately modeled the quasifree response of the nuclei studied, and any deficiency must be highly systematic with mass number. It should be noted that the formalism developed by Smith [32] may be used with more realistic models of the nucleus, and the success of the calculation here certainly indicates that further investigation using such models is warranted.

In summary, the data presented here span the high-mass range of the periodic table and comprise an excellent data set for testing improved calculations of such spectra. These data contain little Gamow-Teller strength due to Pauli blocking and, hence, allow a closer study of spin-isovector excitations of other multipolarities. Spin-isovector dipole strength dominates the spectra of all targets studied here. However, significant spin-isovector monopole strength was found in all targets. The formalism of Smith [32] promises to provide a good calculation of the quasifree cross section. Smith has indicated that improved calculations should include the following.

(a) Inclusion of multistep processes in which the projectile has quasielastic collisions with more than one target nucleon. Smith has shown that the inclusion of such processes can have a large effect on calculations for charge exchange reactions. This is because the charge exchange, involving the isovector part of the NN amplitude, occurs on only one collision, while the other collisions may involve the larger isoscalar amplitude. Further, the different orderings of the collisions must be included, increasing the contribution further.

(b) Collisional damping, which corresponds to the coupling of 1p-1h to many-particle–many-hole configurations through the action of the residual interaction. Unfortunately, the second RPA formalism, which was developed to include this effect, becomes numerically unfeasible except for light nuclei.

(c) The use of an optimal frame in which to evaluate the two-body amplitudes. This simplifies integration over the struck nucleon's momentum, upon which the quasifree cross section should depend. When such a frame is used, the effective laboratory kinetic energy can vary from the true kinetic energy by as much as $\pm 50\%$. Such large variations

will have similarly large effects on energy-dependent amplitudes.

(d) The use of full distorted waves in the calculation of the response.

Any microscopic calculation of charge exchange cross sections must incorporate calculation of the quasifree cross section and should treat collisional damping within the RPA in order to correctly calculate the widths of the resonances.

[1] H. Condé, N. Olsson, E. Ramström, T. Rönnqvist, R. Zorro, J. Blomgren, A. Håkansson, G. Tibell, O. Jonsson, L Nilsson, P.-U. Renberg, M. Österlund, W. Unlelbach, J. Wambach, S. Y. van der Wender, J Ullmannn, and S. A. Wender, Nucl. Phys. **A545**, 785 (1992).

[2] A. Ringbom, A. Håkansson, G. Tibell, R. Zorro, J. Blomgren, H. Condé, J. Rahm, N. Olsson, E. Ramström, T. Rönnqvist, O. Jonsson, L. Nilsson, P.-U. Renberg, S. Y. van der Werf, and H. Lenske, Nucl. Phys. **A617**, 316 (1997).

[3] E. Sugarbaker, D. Marchlenski, T. N. Tadeucci, L. J. Rybarcyk, J. B. McClelland, T. A. Carey, R. C. Byrd, C. D. Goodman, W. Huang, J. Rapaport, D. Mercer, D. Prout, W. P. Alford, E. Gulmez, C. A. Whitten, and D. Ciskowski, Phys. Rev. Lett. **65**, 551 (1990).

[4] A. Klein, W. G. Love, and N. Auerbach, Phys. Rev. C **31**, 710 (1985).

[5] M. Yabe, Phys. Rev. C **36**, 858 (1987).

[6] J. Wambach, S. Drozdz, A. Schulte, and J. Speth, Phys. Rev. C **37**, 1322 (1988).

[7] K. J. Raywood, Ph.D. thesis, University of Melbourne, 1992.

[8] K. J. Raywood, B. M. Spicer, S. Yen, S. A. Long, M. A. Moinester, R. Abegg, W. P. Alford, A. Celler, T. E. Drake, D. Frekers, P. E. Green, O. Häusser, R. L. Henderson, K. H. Hicks, K. P. Jackson, R. G. Jeppesen, J. D. King, N. S. P. King, C. A. Miller, V. C. Officer, R. Schubank, G. G. Shute, M. Vetterli, J. Watson, and A. I. Yavin, Phys. Rev. C **41**, 2836 (1990).

[9] D. F. Osterfield, D. Cha, and J. Speth, Phys. Rev. C **31**, 372 (1985).

[10] J. Wambach, Contemp. Phys. **32**, 291 (1991).

[11] M. A. Moinester, A. Trudel, K. Raywood, S. Yen, B. M. Spicer, R. Abegg, W. P. Alford, N Auerbach, A. Celler, D. Frekers, O. Häusser, R. L. Helmer, R. Henderson, K. H. Hicks, K. P. Jackson, R. G. Jeppesen, N. S. P. King, S. Long, C. A. Miller, M. Vetterli, J. Watson, and A. I. Yavin, Phys. Lett. B **230**, 41 (1989).

[12] R. Helmer, Can. J. Phys. **65**, 588 (1987).

[13] R. S. Henderson, W. P. Alford, D. Frekers, O. Häusser, R. L. Helmer, K. H. Hicks, K. P. Jackson, C. A. Miller, M. C. Vetterli, and S. Yen, Nucl. Instrum. Methods Phys. Res. A **257**, 97 (1987).

[14] R. A. Arndt and L. D. Soper, Phys. Rev. D **35**, 128 (1987).

[15] M. Moinester, Can. J. Phys. **65**, 660 (1987).

[16] W. P. Alford, B. A. Brown, S. Burzynski, A. Celler, D. Frekers, R. Helmer, R. Henderson, K. P. Jackson, K. Lee, A. Rahav, A. Trudel, and M. C. Vetterli, Phys. Rev. C **48**, 2818 (1993).

[17] R. Schaeffer and J. Raynal, computer program DWBA70 (unpublished); J. R. Comfort, extended version DWBA81 (unpublished).

[18] B. A. Brown, computer program PRB (unpublished).

[19] J. Hüfner and C. Mahaux, Ann. Phys. (N.Y.) **73**, 525 (1972).

[20] H. V. von Geramb, F. A. Brieva, and J. R. Rook, Lect. Notes Phys. **89**, 104 (1979); L. Rikus, N. Nakano, and H. V. von Geramb, Nucl. Phys. **A414**, 413 (1984).

[21] H. V. von Geramb, computer program OPMOD (unpublished).

[22] H. De Vries, C. W. Jager, and C. De Vries, At. Data Nucl. Data Tables **36**, 495 (1987).

[23] M. Lacombe, B. Loiseau, J. M. Richard, R. Vinh Mau, J. Cote, P. Pires, and R. de Tourriel, Phys. Rev. C **21**, 861 (1980).

[24] S. El-Kateb, K. P. Jackson, W. P. Alford, R. Abegg, R. E. Azuma, B. A. Brown, A. Celler, D. Frekers, O. Häusser, R. Helmer, R. S. Henderson, K. H. Hicks, R. Jeppesen, J. D. King, K. Raywood, G. G. Shute, B. M. Spicer, A. Trudel, M. Vetterli, and S. Yen, Phys. Rev. C **49**, 3128 (1994).

[25] M. C. Vetterli, O. Häusser, R. Abegg, W. P. Alford, A. Celler, D. Frekers, R. Helmer, R. Henderson, K. H. Hicks, K. P. Jackson, R. G. Jeppesen, C. A. Miller, K. Raywood, and S. Yen, Phys. Rev. C **40**, 559 (1989).

[26] R. Leonardi, E. Lipparini, and S. Stringari, Phys. Rev. C **35**, 1439 (1987).

[27] A. Errel, J. Alster, J. Lichtenstadt, M. A. Moinester, J. D. Bowman, M. D. Cooper, F. Irom, H. S. Piasetzky, and U. Sennhauser, Phys. Rev. C **34**, 1822 (1986).

[28] J. Lisantti, J. R. Tinsley, D. M. Drake, I. Bergqvist, L. W. Swenson, D. K. McDaniels, F. E. Bertrand, E. E. Gross, D. J. Horen, and T. P. Sjoren, Phys. Lett. **147B**, 23 (1984).

[29] H. Esbensen and G. F. Bertsch, Ann. Phys. (N.Y.) **157**, 255 (1984).

[30] R. D. Smith and J. Wambach, Phys. Rev. C **36**, 2704 (1987).

[31] R. D. Smith and J. Wambach, Phys. Rev. C **38**, 100 (1988).

[32] R. D. Smith, in *Spin Observables In Nuclear Probes*, edited by C. J. Horowitz, C. D. Goodman, and G. E. Walker, IUCF Conferences at Telluride (Plenum, New York, 1988).

[33] M. H. Macfarlane, Can. J. Phys. **65**, 626 (1987).

[34] R. D. Lawson, *Theory of the Nuclear Shell Model* (Clarendon, Oxford, 1980).

[35] D. M. Brink and G. R. Satchler, *Angular Momentum*, 2nd ed. (Oxford University Press, New York, 1979).

[36] K. Bleuler, M. Beiner, and R. de Tourreil, Nuovo Cimento B **52**, 45 (1967); **52**, 149 (1967).

[37] M. A. Franey and W. G. Love, Phys. Rev. C **31**, 488 (1985).

[38] H. V. von Geramb, in *The Interaction Between Medium Energy Nucleons in Nuclei*, edited by H. O. Meyer, AIP Conf. Proc. No. **97** (AIP, New York, 1983), p. 44.

[39] R. D. Smith (unpublished).